Journal of Neural Engineering

PAPER

Residual voltage as an ad-hoc indicator of electrode damage in biphasic electrical stimulation

Ashwati Krishnan[1,*], Mats Forssell[1], Zhanhong Du[2], X Tracy Cui[3], Gary K Fedder[1] and Shawn K Kelly[4,5]

[1] Department of Electrical and Computer Engineering, Carnegie Mellon University, Pittsburgh, PA 15213, United States of America
[2] Shenzhen Institute of Advanced Technology, Shenzhen City, Guangdong, People's Republic of China
[3] Department of Bioengineering, University of Pittsburgh, Pittsburgh, PA 15213, United States of America
[4] VA, Pittsburgh, PA 15240, United States of America
[5] Institute of Complex Engineered Systems, Carnegie Mellon University, Pittsburgh, PA 15213, United States of America
[*] Author to whom any correspondence should be addressed.

E-mail: krishnan.cmu@gmail.com

RECEIVED
14 September 2020

REVISED
27 February 2021

ACCEPTED FOR PUBLICATION
18 May 2021

PUBLISHED
12 August 2021

Keywords: residual voltage, electrode-tissue interface, electrical stimulation, electrode health monitoring, electrode damage detection, biphasic current stimulation

Abstract

Objective. We derive and demonstrate how residual voltage (RV) from a biphasic electrical stimulation pulse can be used to recognize degradation at the electrode-tissue interface. *Approach.* Using a first order model of the electrode-tissue interface and a rectangular biphasic stimulation current waveform, we derive the equations for RV as well as RV growth over several stimulation pulses. To demonstrate the use of RV for damage detection, we simulate accelerated damage on sputtered iridium oxide film (SIROF) electrodes using potential cycling. RV measurements of the degraded electrodes are compared against standard characterization methods of cyclic voltammetry and electrochemical impedance spectroscopy. *Main results.* Our theoretical discussion illustrates how an intrinsic RV arises even from perfectly balanced biphasic pulses due to leakage via the charge-transfer resistance. Preliminary data in *in-vivo* rat experiments follow the derived model of RV growth, thereby validating our hypothesis that RV is a characteristic of the electrode-tissue interface. RV can therefore be utilized for detecting damage at the electrode. Our experimental results for damage detection show that delamination of SIROF electrodes causes a reduction in charge storage capacity, which in turn reflects a measurable increase in RV. *Significance.* Chronically implanted electrical stimulation systems with multi-electrode arrays have been the focus of physiological engineering research for the last decade. Changes in RV over time can be a quick and effective method to identify and disconnect faulty electrodes in large arrays. Timely diagnoses of electrode status can ensure optimal long term operation, and prevent further damage to the tissue near these electrodes.

1. Motivation

High-density microelectrode arrays are becoming the norm for neuromodulation devices, in applications such as retinal implants and cortical stimulators. When microelectrode arrays are chronically implanted in tissue for stimulation, a multitude of mechanisms can affect their performance. Animal tissue environments are responsive to the presence of a foreign entity, often causing lesions due to implantation of the device, leading to loss and subsequent remodeling of neural tissue, thereby reducing electrode performance [1]. In 2013, Barrese *et al* analyzed long term failure modes of intracortical microelectrode arrays on 27 non-human primates for a period of five years [2]. It was found that 56% of microelectrode failures occurred within a year of implantation. An early increase in impedance, followed by a slow decline due to failure of insulating material was also observed. While the stimulation electrode may be effective over acute time periods, the prolonged use of chronically implanted electrodes

often exhibit unwanted responses. Some of the mechanisms that contribute to electrode-tissue interface damage on prolonged use include:

- a change in the electrochemical impedance due to a barrier following encapsulation of fibrous growth,
- movement of electrodes from the implantation site,
- mechanical breakage (or delamination) of the electrode,
- effects of neural plasticity around the electrode [3],
- changes in the stimulation electrode characteristics due to electrode dissolution [4].

Because the number of electrodes in multi-electrode arrays can be of the order of 1000 or higher, the problem of identifying functional electrode sites from degraded ones becomes warranted and challenging. Although an understanding of electrode geometry and material as well as stimulus input is required to ensure safe stimulation, they are not sufficient to predict electrode or tissue damage. A review published by Cogan *et al* in 2016 [5], suggests that the performance of stimulation microelectrodes do not necessarily adhere to the existing norms of stimulation parameters, namely charge per phase and charge density, as suggested in the Shannon equation [6]. It is advantageous to analyze each damaged/degraded electrode individually through standard electrochemical methods, however, these processes do not scale well because (a) they are time consuming and (b) they involve sizeable instrumentation. If we can diagnose the problem *early* by measuring residual voltage (RV) during stimulation, then we can disconnect any sub-standard electrode before unpredictable, possibly detrimental changes can occur at the electrode-tissue interface. The research presented in this paper establishes the concept, applicability and evidence of measuring RV after a biphasic stimulus, as a way of detecting any changes to the electrode/electrolyte (tissue) interface in a chronic stimulation implanted electrode. We first present a background, derivation and definition of RV in biphasic electrical stimulation in section 2 and a technical discussion of why it is advantageous to use this method of stimulation and RV measurement for damage detection in section 3. The remainder of the paper outlines rigorous experimental evidence, both *in vitro* and *in vivo*. We present results of RV growth over time in the absence of good charge balancing methods, creating unsafe operating points for stimulation and also conclude that a drastic increase in RV corresponds to reduction in charge storage capacity of stimulation electrodes.

2. Residual voltage in biphasic current stimulation

Electrical stimulation for neural prosthesis devices is typically performed using biphasic pulses. Balanced biphasic waveforms were first introduced as a safe method of stimulation by Lilly *et al* in 1955 [7]. Artificial triggering of an action potential can be achieved by voltage stimulation, current stimulation, and more recently switched capacitor stimulation [8] and high frequency current-switching stimulation [9]. For stimulation electrode materials that involve Faradaic reactions, a charge balanced waveform ensures that electrochemical reactions that occur in the first phase, are reversed in the second phase, ensuring a net zero injection of charge into tissue for safety. While voltage stimulation is more power efficient [10], we cannot control the amount of charge that is being delivered into the tissue because the load draws as much current as it requires. The electrode–electrolyte/tissue interface is not a constant or deterministic load, therefore voltage stimulation is not a safe option in dynamic electrode-tissue environments. Therefore, biphasic *current* stimulation has become the *de facto* standard because charge delivery can be controlled more efficiently for loads where the impedance varies over time.

2.1. Biphasic current stimulation

Biphasic current stimulation waveforms are electric current stimulus signals, typically rectangular waveforms, that consist of a stimulation phase, an interphase delay, followed by a recovery phase (figure 1(a)). The *stimulation* phase is the phase that elicits the action potential in the neuronal cell. The *recovery* phase is used to neutralize the charge sent in the first phase. The stimulation phase of biphasic waveforms is usually cathodic because it is more efficient in eliciting an action potential from an excitable cell [11]. The recovery phase is the anodic phase, used to electrically neutralize the charge injected by the cathodic phase, after the generation of the action potential. The *interphase delay* is a period with zero stimulation between the stimulation and recovery phase. The interphase delay is believed to allow the action potential to propagate before charge recovery, although there is ongoing research to study the effects of interphase delay on stimulation [12, 13]. If the total charge injected in the stimulation phase equals the total charge in the recovery phase, i.e. $|Q_c| = |Q_a|$, then the stimulation is said to *balanced*. The mismatch in charge between the cathodic and anodic phases in a biphasic stimulation pulse is termed as the *biphasic mismatch error*. The magnitude and duration of the current pulse depends on the physiology of the target tissue and the application [14]. A generic current-based, cathodic-first, square, biphasic stimulation waveform is shown in figure 1(a).

Normal experimental conditions in this work are based on safe stimulation of target retinal ganglion cells through a 400 μm diameter sputtered iridium oxide film (SIROF) electrode [10]. These cells respond to a maximum stimulation current of 100 μA, with initial pulse widths of 1 ms with an interphase delay of 100 μs. Residual voltage in

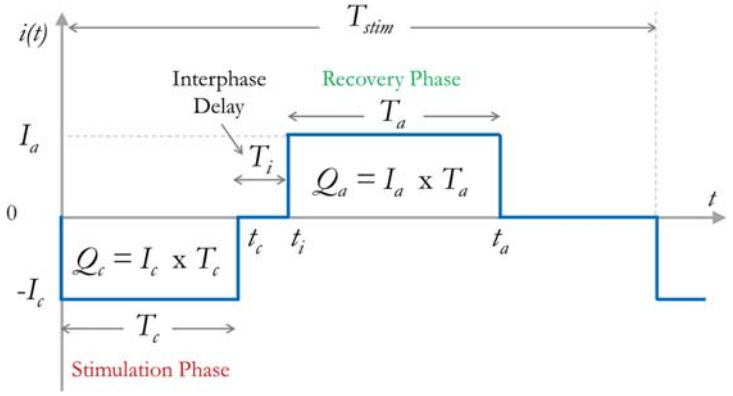

(a) Current-based Biphasic Stimulation Waveform

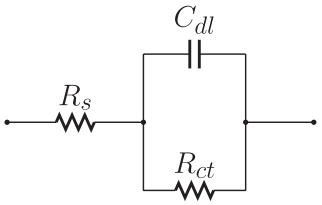

(b) First order model of electrode tissue interface

Figure 1. (a) Biphasic current stimulation waveform: Biphasic waveforms are said to be *balanced* when $|Q_c| = |Q_a|$. In this work, the stimulation phase is assumed to be cathodic (negative) and the recovery phase is anodic (positive). T_c, T_i and T_a are cathodic, interphase and anodic pulse *widths*. Stimulation time period is given by T_{stim}. Absolute time is denoted by t_c, t_i, t_a. The magnitude of cathodic current is expressed as I_c, and anodic current by I_a (b) First order electrode-tissue interface model: R_s is the solution resistance, R_{ct} is the charge-transfer resistance and C_{dl} is the double-layer capacitance. The relaxation time constant is $\tau = C_{\text{dl}} \times R_{\text{ct}}$.

biphasic current stimulation can be observed after a biphasic current pulse passes though an electrode–electrolyte interface. For the theoretical discussions in this work, we assume the first order model of the electrode–electrolye (tissue) interface [15], shown in figure 1(b), is being driven by biphasic current pulses. The notations used in this paper are described under figure 1.

2.2. Origin of residual voltage

RV is an accumulation of charge that manifests as a voltage when biphasic current pulses are applied across an electrode–electrolyte interface. Consider the biphasic current stimulation pulse (figure 1(a)), applied across the electrode–electrolyte model shown in figure 1(b). For a *balanced* biphasic current pulse (figure 2), the cathodic phase of the biphasic current pulse negatively charges the double-layer capacitance, C_{dl}, and the *balanced* anodic phase discharges the capacitor. Observe from figure 2, that the double layer capacitance is nearly always negatively charged (because the stimulation pulse is cathodic-first). Consequently, in the presence of the charge-transfer resistance, R_{ct}, there is a *unidirectional* leakage across R_{ct} for most of the duration of the stimulation pulse, even if the phases of the stimulation pulse are perfectly balanced [16]. Therefore, there will be a non-zero RV present at the end of the pulse even with balanced biphasic pulses if R_{ct} is included in the model.

For the notations described in figure 1(a), the RV at the end of the anodic pulse width, in terms of the biphasic stimulation pulse-widths is:

$$v_c(t_a+) = -I_c R_{\text{ct}}[e^{-(T_i+T_a)/\tau} - e^{-(T_c+T_i+T_a)/\tau}] + I_a R_{\text{ct}}[1 - e^{-(T_a)/\tau}]. \quad (1)$$

In particular, for a *balanced* biphasic waveform, if $|I_c| = |I_a| = I$ and $T_c = T_a = T$, (1) reduces to an expression that has a non-zero value at the end of the anodic pulse as shown in (2), which implies that there exists an *intrinsic* RV,

$$v_c(t_a+)_{\text{intr}} = IR_{\text{ct}}\left[1 - e^{-(T_i+T)/\tau} + e^{-(2T+T_i)/\tau} - e^{-(T)/\tau}\right]. \quad (2)$$

While this is a first order model of the electrode–electrolyte interface, it allows us to understand the characteristics of the RV, with respect to the electrode model parameters. The expression for RV in biphasic current stimulation for a first-order model shown in (1) is the voltage that appears at the end of the *first* pulse. In practice, several stimulation pulses are continuously applied, the following section describes the development of the model equation for RV growth.

2.3. RV growth

In the absence of charge control methods, the RV will grow over time, as can be extrapolated from the charging of the capacitor in figure 1(b). The time

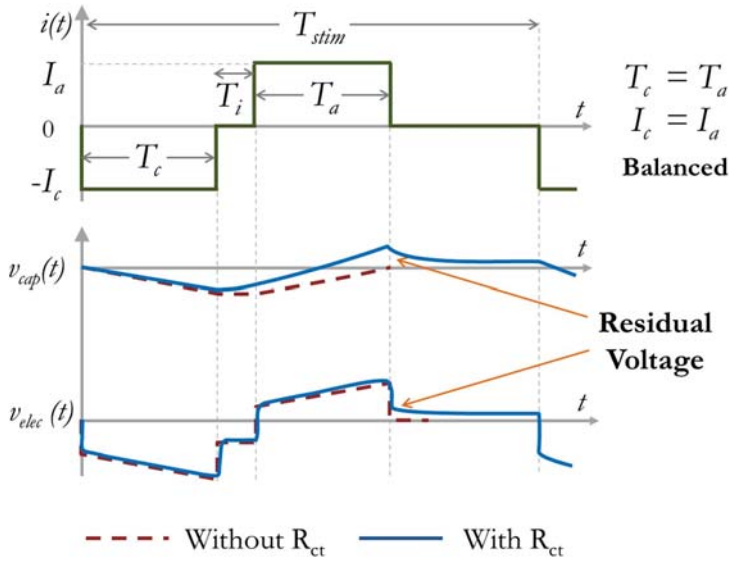

Figure 2. Schematic representation of RV arising from balanced biphasic stimulation. The dashed line shows the voltage across C_{dl} if R_{ct} was not present in the model (there would be no leakage). Balanced biphasic pulses have zero biphasic mismatch, i.e. $Q_c = Q_a$, and unidirectional leakage across R_{ct} occurs even with zero biphasic mismatch.

required for the double-layer capacitance to completely discharge is theoretically infinite, the time constant of discharge via the charge transfer resistance is $\tau = R_{ct} \times C_{dl}$, called the *relaxation time constant [17]*. If the frequency of the stimulation pulse is low, then there is negligible net RV growth. Without charge balancing, the stimulation electrode will operate at different bias voltages, higher bias voltages being potentially harmful. Therefore, it is of interest to theoretically understand the model of RV growth in a stimulation electrode over several stimulation pulses.

As a more general case, the RV including the effects of the intrinsic leakage, as well as biphasic mismatch at the end of the anodic pulse of the first biphasic waveform, RV_0, is shown in (1). This voltage discharges for the time after the anodic pulse, until the next biphasic stimulation pulse,

$$RV_0 = \mathrm{RV}|_{T_a}.\exp\left(-\frac{T_{\mathrm{stim}} - t_a}{\tau}\right). \tag{3}$$

If we follow through the differential equation (3) assuming the same input waveform for the next biphasic stimulation pulse, we get the discharged RV to be,

$$RV_1 = RV_0 + RV_0 e^{\frac{-T_{\mathrm{stim}}}{\tau}}. \tag{4}$$

By recursively applying (4) for subsequent stimulation pulses, with the same input biphasic stimulation pulse, we get

$$RV_n = RV_0 \left[1 + e^{\frac{-T_{\mathrm{stim}}}{\tau}} + e^{\frac{-2T_{\mathrm{stim}}}{\tau}} + \ldots + e^{\frac{-nT_{\mathrm{stim}}}{\tau}}\right]. \tag{5}$$

The value of the stimulation time period, T_{stim}, is typically 10 ms and the relaxation time constant, τ, of a stimulation electrode can be of the order of 20 ms or higher [10]. Therefore, (5) can be solved as a sum of a geometric series, where the common factor is $\exp(\frac{-T_{\mathrm{stim}}}{\tau})$, which under practical values will be less than 1. The sum of n terms for such a series will converge to,

$$RV_n = RV_0 \frac{1 - (\exp(-T_{\mathrm{stim}}/\tau))^{n-1}}{1 - \exp(-T_{\mathrm{stim}}/\tau)}, \tag{6}$$

which as $n \to \infty$,converges to,

$$RV_{\mathrm{sat}} = \lim_{n\to\infty} RV_n = RV_0 \left[\frac{1}{1 - \exp\left(\frac{-T_{\mathrm{stim}}}{\tau}\right)}\right]. \tag{7}$$

From (7), we observe that the RV saturates, and that the saturated RV depends on the stimulation frequency and the relaxation time constant. One consequence of a saturated RV is that it dynamically changes the operating point of the stimulation electrode. The RV growth saturation in (7) combines contribution from charge mismatch in the two phases, as well as leakage via the charge-transfer resistance. However, it should be noted that charge mismatch is a systematic error that arises due to electronic inefficiencies, and can be characterized or calibrated prior to stimulation. Any changes to the structure of the electrode itself will be reflected in the charge-transfer resistance, which in turn is captured by deviations from the initial RV measurement. Having developed first-order theoretical models for RV and the extent of its growth, we outline in section 3 the reasons which make the measurement of RV after biphasic stimulation an efficient, ad-hoc method to monitor electrode damage in high density stimulation arrays.

3. Why use RV for damage detection?

There are several advantages to using RV as an early indicator of electrode damage: firstly, the RV is one of the most accessible measurements that is a function of R_{ct} and C_{dl}. The reason it is easily accessible is because it does not require additional electrodes, only a simple sampling at a non-critical period of the stimulation waveform i.e. it does not require an interruption during stimulation. Secondly, the measurement is performed *after* the stimulation pulse. Because the stimulation frequency of most applications is of the order of 100 Hz, state of the art microelectronics can acquire fairly accurate samples at frequencies that are greater by at least two orders of magnitude. Thirdly, the dynamic range for detection of RV is smaller than that required for measuring the entire stimulation waveform. RV values after a biphasic stimulation pulse range in the order of a few millivolts, as opposed to solution resistance (R_s) measurements, which can be in the order of volts. This makes it easier to develop low-power hardware circuits for the measurements.

One of the more popular and established mechanism for guaranteeing safety in an electrode is to short-circuit the electrode immediately after stimulation. The shorting mechanism uses a switch to bypass any residual charge in the form of current away from the electrode after the stimulation is complete. When the shorting switch is active, the voltage on the electrode will be clamped at zero, to keep it at a safe level.The elegance of the shorting method lies in its simplicity, because the electronic switch is one of the most inexpensive pieces of hardware that could be added to a circuit. However, the method is brute-force, and it nulls a voltage measurement that may give us a clue about the health of the interface. To combat this, our work in this paper suggests that one can sample the RV and then short the electrode. There are other ways of charge balancing [18] to ensure zero RV including using DC block capacitors and long term offset regulation [19]. However, using these methods may prevent us from obtaining real time information about early damage in implanted electrodes. Cogan *et al* suggest an alternative method of measuring the electrode voltage during the interphase pulse as a direct measure of the voltage across the double layer capacitance [20]. While a measure of a charged C_{dl} is very beneficial, the order of biphasic interphase pulse widths is around 100 μs and the voltage across the capacitance may be 0.5 V, depending on the size and material of the electrode. These constraints make the design of electrode measurement circuits less scalable and energy inefficient. In an *in vitro* tissue study performed by Merrill and Tresco [3], it was found that the variation of electrode impedance with different biological cell cultures *in vitro* increased 20%–80% from the measured value before contact with the cultures, which is a broad range. RV measurements provide an indication of whether the stimulation circuit 'sees' the same load circuit as it was designed for. If there is any change, the stimulation system can be designed to shut down or adapt to a different configuration.

In this work, we demonstrate methods of RV measurement before and after degradation of Sputtered Iridium Oxide Film (SIROF) electrodes in phosphate buffered saline (PBS). The following steps were used to validate the measurement of RV from biphasic stimulation as a method to detect evidences of change at the electrode–electrolyte (tissue) interface.

(a) Characterization of electrodes using cyclic voltammetry (CV) and electrochemical impedance spectroscopy (EIS) before break-in
(b) Break-in of SIROF electrodes[6], followed by re-characterization
(c) Measurement of RV using a biphasic current stimulator with known mismatch
(d) Characterization of electrodes using CV and EIS and RV
(e) Comparison of characterization data with RV measurements with CV and EIS measurements

This procedure was followed both in preliminary *in vivo* experiments in rats, as well as in a simulated systematic process to mimic degradation, so that RV can be studied in more samples. Section 4 describes the setup and characterization methods used in this work. Section 5 illustrates preliminary *in vivo* experimental evidence of RV growth. We corroborate our RV measurement data with CV and EIS. Our results in section 7 show that delaminated electrodes exhibited an increase in measured RV after biphasic electrical stimulation [21].

4. Characterization methods

The electrochemical setup used in this work (figure 3) comprised the SIROF working electrode in an array of 15 electrodes (figure 3(a)) and a coiled platinum (Pt) counter electrode in 1X phosphate buffered saline (PBS) solution. PBS is an isotonic buffer solution used in biological research because the osmolarity, pH and ion concentrations match those of the human body. A three electrode setup was used for cyclic voltammertry (CV) and electrode impedance spectroscopy (EIS) experiments performed using PGSTAT302N potentiostat (Metrohm Autolab, The Netherlands), with an Ag/AgCl reference electrode (Basi Inc. MF2052) to characterize the electrode array (figure 3(b)). The area of each SIROF (working)

[6] A commonly accepted process of activation for sputtered iridium oxide film (SIROF) electrodes prior to regular use.

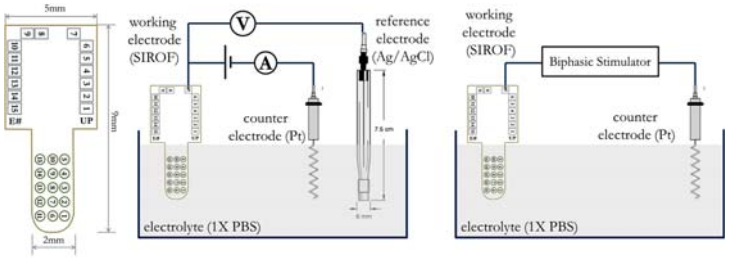

Figure 3. Experimental setup for RV validation experiments: (a) SIROF working electrode array of 15 electrodes obtained from [22] with each electrode of 400 μm diameter. The working electrode array was bonded to a circuit breakout board using cellophane tape, and sealed in a container using silicone glue. (b) Simplified three electrode measurement setup for Autolab Metrohm (c) Two electrode measurement setup for stimulation. The counter electrode (Basi Inc. MW1033) is made of platinum and has a surface area 2000 times the area of the SIROF electrode, which is sufficient to neglect any potential changes across the counter electrode.

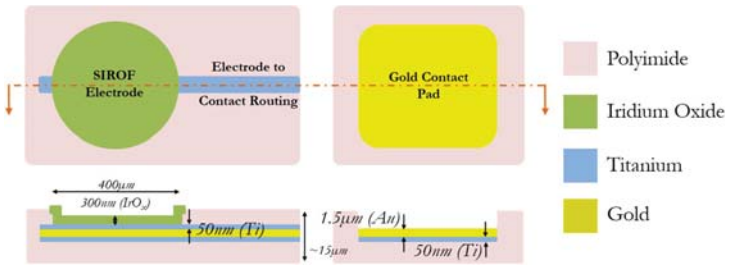

Figure 4. Schematic cross section of a SIROF electrode, which has a diameter of 400 μm. The gold contact pads have an edge of 250 μm. Titanium is used as an adhesion layer, with a polyimide base structure (image adapted from [22] and not drawn to scale).

electrode is approximately 2000x smaller than the platinum counter electrode used in the setup, therefore, charge accumulation at the counter electrode is assumed to be negligible when compared to the working electrode. Therefore, practical electrical stimulation and subsequently, RV measurements, employ a two electrode (figure 3(c)) setup.

4.1. Electrode material

Faradaic materials such as SIROF electrodes were developed to achieve higher charge injection capacities [23]. The SIROF electrodes used in this work were developed by Shire *et al* at Cornell University as part of the Boston Retinal Implant Project. The details of the fabrication process of the electrodes are described in [22]. A schematic cross section of the sputtered iridium film electrodes used in this work is shown in figure 4.

The polyimide based electrode array, containing 15 electrode sites, was first lifted-off from its silicon substrate. Once removed, the array was adhered to a circuit breakout board using cellophane tape, such that the contacts on the array aligned with the contacts on the board. In order to hold the electrode in place with respect to the circuit board, a 3D printed clamp was used to press the electrode against the circuit board. The clamp was sealed in silicone to prevent seepage of saline through capillary effect under the electrode, which can cause shorting of electrode pads.

Table 1. Typical CV and EIS parameters for electrochemical characterization.

CV parameter	Value
Scan rate	0.1 V s^{-1}
Lower potential limit (V_L)	−0.6 V
Upper potential limit (V_H)	+0.8 V
# Zero crossings	6
EIS parameter	**Value**
Sinusoidal input	10 mV$_{RMS}$
Lower frequency limit	0.1 Hz
Upper frequency limit	100 kHz
# Frequency values	50

4.2. Preparation & break-in SIROF electrode array

The electrodes are characterized prior to first use using CV and EIS with a three-electrode measurement setup. The parameters used for typical CV and EIS characterizations are described in table 1.

After initial characterization, the electrodes were subject to potential cycling (repeated CV cycles) to activate the iridium oxide film. Activation by means of repeated CV measurements causes the initial layer of iridium oxide to become extended as a thicker, hydrated oxide [24]. The CV cycles were performed at a scan rate of 0.1 V s^{-1}, between the limits of −0.6V/+0.8V [23] for 14 min. For these experiments,

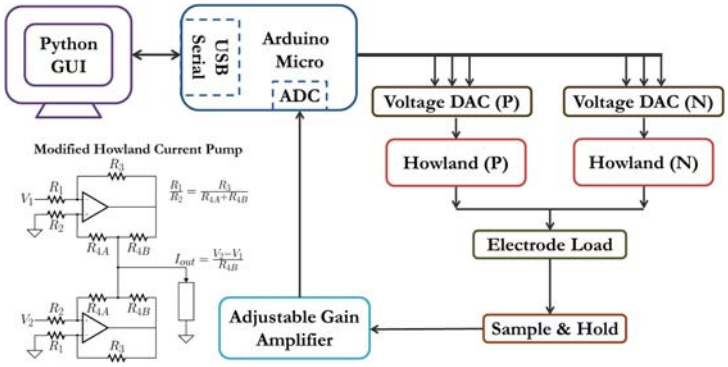

Figure 5. Schematic block diagram of the BiCAF board: A voltage DAC operated modified Howland current source with a modified Howland current pump circuit, designed to accommodate bidirectional current, with the capability of supplying different current ranges based on the power supply, and resistor values.

the number of zero-crossings was adjusted to set the duration of the CV cycling. Of the 15 electrodes present in the electrode array, 13 electrodes were prepared for use and characterized using CV and EIS (figure 3(a)).

4.3. Biphasic stimulation responses

To study the effects of RV across the electrode–electrolyte interface, a programmable stimulator was designed and developed in our lab. The biphasic current stimulator with active feedback (BiCAF) board is a programmable, controllable high impedance biphasic current source (figure 5) with provision to implement active feedback algorithms in neural stimulation systems. The components of the board can be modified to suit different magnitudes of current. The RV measurement is sampled using the LF398 integrated circuit, which is a sample and hold integrated circuit with an input impedance of $10^{10}\Omega$. The sampled voltage is sent to the analog-to-digital converter present in the Arduino Micro. The Arduino Micro is an open-source, cross-platform microcontroller (ATmega32u4) board, controls the functionality of the system and interfaces with the PC via a serial USB protocol. The stimulation system parameters can be adjusted via a Python-based graphic user interface. The default stimulation parameter values that were used for experimentation are shown in table 2.

All the electrodes were driven by closely balanced biphasic pulses at 100 Hz generated by the BiCAF system. Transient responses for one pulse were measured with a 10 MΩ, 14pF probe on a DSO7012B oscilloscope (Keysight, CA, USA) with a minimum sampling rate of 20kS/s, the data was smoothed in MATLAB (Mathworks, MA, USA) using a moving average filter.

4.4. Data from characterization measurements

4.4.1. Cathodal charge storage capacity

The charge capacity of an electrode is used as a measure of the maximum charge that can be injected into the electrolyte through the electrode [23]. The cathodal charge capacity was obtained by numerically integrating the current under the negative half of the CV curve, and dividing it by the area of the electrode. The units of cathodal charge capacity are reported as coulombs per square centimeter (C cm^{-2}).

Table 2. BiCAF performance parameters.

System block	Parameter	Value
Power supply	Dual power supply	$> \pm 10$ V
	Min. voltage compliance	2.5 V
Current source	Current DAC resolution	8 bit
	Pulse rise/fall time	10 μs
	Pulsewidth resolution	1 μs
	Max. current amplitude	± 100 μA
	Biphasic charge mismatch	1.5%
Microcontroller	Clock frequency	16 MHz
	ADC conversion time	< 250 μs
	ADC resolution	10 bit
	Min. voltage measurement resolution	1mV

4.4.2. Impedance

The magnitude and phase of EIS plots were recorded for all the electrodes. The low frequency impedance on the magnitude plot provides a lower bound of $(R_s + R_{ct})$ values. The high frequency impedance is a measure of the solution resistance, R_s. In this work we have assumed a simplified electrode–electrolyte (tissue) model (figure 1(b)) to illustrate the existence and application of RV in biphasic stimulation. While a detailed description and extraction of the impedance parameters is beyond the scope of this work, we have provided complete impedance plots to illustrate the deviation of impedance and RV when subject to the simulated electrode degradation protocol.

Using the methods outlined above, we performed acute, preliminary *in vivo* experiments in rats to see if RV growth followed the model we derived in

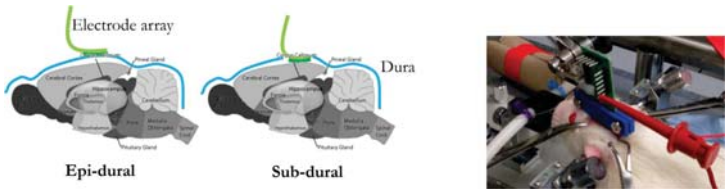

(a) Schematic of SIROF Electrode Placement (b) Photograph of *in-vivo* Setup

Figure 6. (a) Schematic of epidural and subdural SIROF electrode mounting in SD rat (b). Epidural placement is above the dura, while sub-dural is under the dura. Photograph of the electrode array mounted on a Sprague-Dawley rat. The location was chosen based on ease of surgical accessibility of the neural tissue.

section 2, and understand what effects uncontrolled RV growth can have at the electrode–tissue interface.

5. Evidence of RV in experiments *in vivo*

Experiments performed in physiological PBS allow us to mimic passive chemical environments and the dielectric properties of biological interfaces. To develop effective dynamic neural stimulators, it is imperative to observe the active nature of the electrode-tissue interface. There has been no evidence in prior work showing how high the RV growth can be *in vivo* tissue. We present the results of a preliminary experiment on RV growth in the brain tissue of a live anesthetized rat. The purpose of the experiment was to observe the how high the RV can go to in neural tissue and observe the effects of RV *in vivo*. We observed the incidence and growth of RV, and characterized the electrode-tissue interface *in vivo*.

All the experimental and surgical procedures were approved by the Institutional Animal Care and Use Committee (IACUC) at the University of Pittsburgh, and were in compliance with the US Public Health Service policy on the human care and use of laboratory animals. We used one Sprague-Dawley rat, which was anesthetized for the duration of the experiment. A craniotomy was performed to expose the *dura-mater*. The SIROF electrode array (figure 3(a)) was mounted in two locations, epidural and subdural (figure 6(a)). The electrode was placed near the visual cortex. A platinum counter electrode was placed near the working electrode. To prevent the tissue from drying, the environment is flushed with saline solution. A photograph of the experimental setup is shown in figure 6(b). The stimulation parameters used for these experiments are the same as those specified in table 3.

The electrode-tissue interface characteristics were measured using CV and EIS using the Metrohm Autolab equipment before and after prolonged exposure to RV at the epidural and subdural electrode locations. RV growth was observed in saline solution for approximately 60 min, in the epi-dural location for 35 min and in the sub-dural location for 15 min. The RV growth curves for the epi-dural, sub-dural and saline cases are shown in figure 7(c). A significant result from this work is the evidence that the RV can grow beyond the water window limits (for SIROF electrodes). The RV growth model derived in section 2.3 appears to be valid in the case of *in-vivo* tissue.

Table 3. Stimulation parameter values.

Parameter	Symbol	Typical value
Stimulation frequency	$F_{stim} = 1/T_{stim}$	100 Hz
Cathodic pulse width	T_c	1000 μs
Anodic pulse width	T_a	1000 μs
Interphase delay	T_i	100 μs
Cathodic current amplitude	I_c	100 μA
Anodic current amplitude	I_a	100 μA

The electrode-tissue interface was characterized using CV and EIS before and after exposure to the RV growth, for both the epi-dural (35 min) and the sub-dural locations (15 min), shown in figures 8, 9(a) and (b).

5.1. Discussion

The *in vivo* experiments performed as part of this work give a very practical idea of the nature of RV and whether we need to be concerned about its existence and growth in real animal tissue. The RV growth curves between cases *in vivo* and *in vitro* along with a model fit done using the Curve Fitting Tool in MATLAB is shown in figure 7(c).

The time constant shown in the plot refers to the relaxation time constant, and the RV growth equation used for the model fit is based on (7). There are three main observations from the plot: (a) the relaxation time constant is higher for the *in-vivo* cases and (b) the final value of the voltage is higher in the *in vivo* cases and (c) the final value is higher than the water window limits for the SIROF electrode. The increase in time constant and steady-state voltage is explained by an increase in either the double-layer capacitance (C_{dl}) or the charge-transfer resistance (R_{ct}), or both. Observe from (2) that the voltage at the end of the anodic pulse of a biphasic stimulation pulse contains

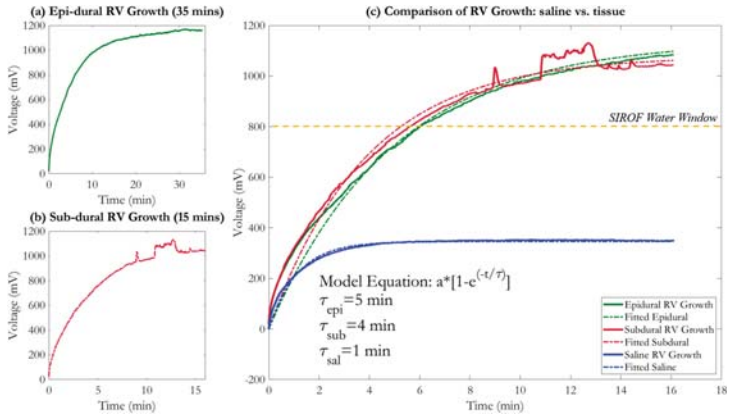

Figure 7. RV growth curves *in vivo*: (a) RV growth in the epi-dural location, recorded for 35 min (b) RV growth in the sub-dural location, recorded for 15 min (c) comparison of *in-vivo* tissue RV growth with *in vitro* saline RV growth. The RV growth crosses the water window limits *in vivo* tissue, resulting in a potentially unsafe environment for chronic stimulation. RV growth *in vivo* model fit: the model fit using the exponential model equation shows that the relaxation time constant ($\tau = C_{dl} \times R_{ct}$) of the curves *in vivo* are larger than the case in saline.

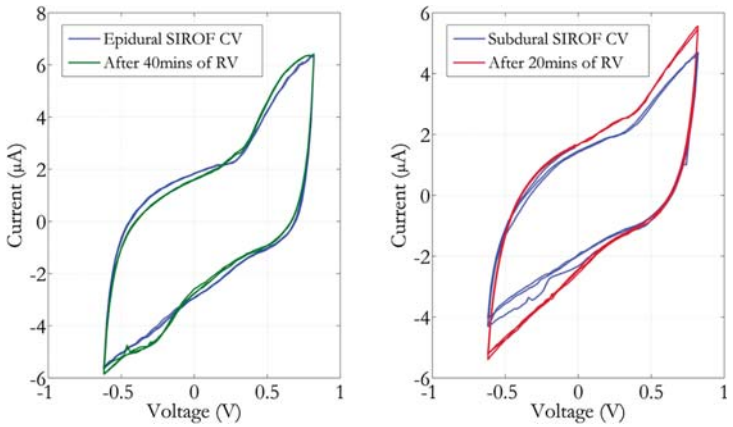

Figure 8. CV curves after prolonged exposure to RV *in vivo*, shows a slight increase in the charge storage capacity, but not as significant.

the parameters R_{ct} and C_{dl}, which captures information about the electrode–electrolyte interface, and not just the biphasic mismatch error between anodic and cathodic pulses. This preliminary *in vivo* experiment, validated by a first–order model equations show that monitoring of RV can provide early information about the status of a stimulation electrode in tissue. We proceed to elaborate on the relevance of using RV to examine the state of the electrode–tissue interface during stimulation.

6. Simulated degradation

6.1. Electrode degradation protocol

The main objective of this paper is the idea that one can use RV from biphasic current stimulation, as an ad-hoc indicator of changes at the electrode–electrolyte interface. The basis of using RV measurements and subsequent applications are outlined in section 3. From the standpoint of high–density stimulation electrode systems, if there is any indication of damage at any one of the electrode interfaces, a timely RV measurement can ensure that the damaged channel can be disconnected to avoid further problems.

In order to validate the usefulness of measuring the RV, the approach followed in this work is to systematically and repeatably degrade stimulation electrodes and measure the RV. There is empirical evidence that exposing SIROF electrodes above the electrochemical water window limits of −0.6 V/+0.8 V, causes damage to the film [23]. We have shown in section 5 that these limits can indeed be reached if RV growth is not controlled. Using the water window limits as a premise *to trigger degradation*, the electrodes were subject to CV cycling at limits that are *above* −0.6V/+0.8V, each for a duration of 1 h, in 1X PBS. The values of zero crossings in table 4 are adjusted to make sure all the electrodes are exposed to the saline under each condition for the same duration of 1 h. The duration was empirically chosen to ensure that different

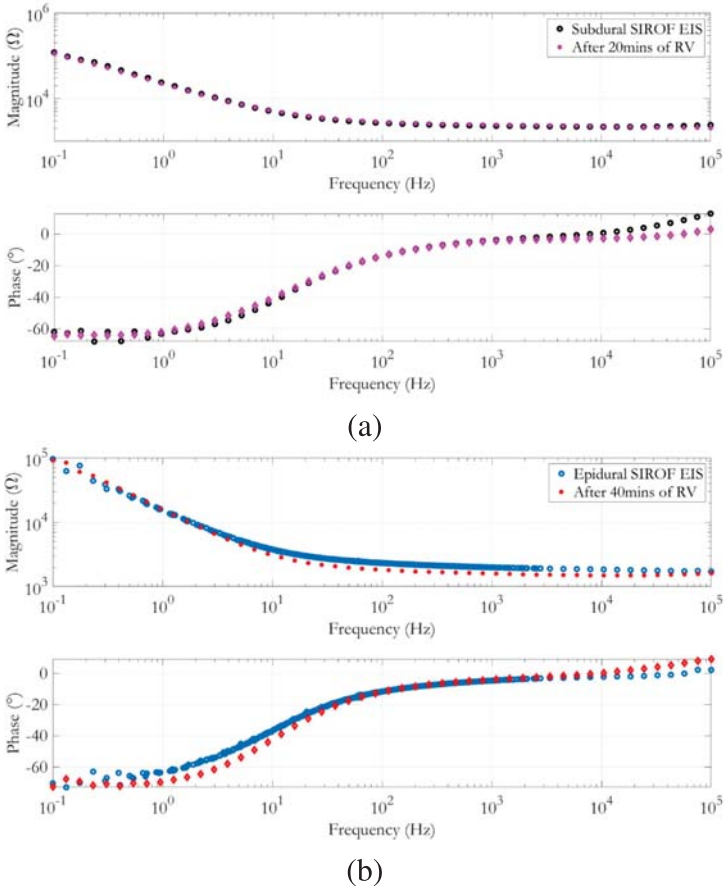

Figure 9. (a) Subdural EIS after 20 min of prolonged RV exposure (b) epidural EIS after 40 min of prolonged RV exposure.

Table 4. Degradation protocol using CV.

Degradation protocol	Electrodes #	V_L	V_H	# Zero crossings	Deviation from water window (WW)
I	5,10,15	−0.4 V	+0.6 V	360	Within WW
II	3,4,6	−0.6 V	+0.8 V	257	At WW
III	7,8,9	−1.2 V	+1.4 V	200	Above WW by $\|0.6V\|$
IV	12,13,14	−1.6 V	+1.8 V	105	Above WW by $\|1V\|$
V	11	−1.8 V	+2.0 V	100	Above WW by $\|1.2V\|$

Degradation protocol using CV, by using the potential limits for the CV measurement above water window limits for SIROF [23]. The electrode numbers are based on the numbers marked in figure 3(a). V_H and V_L are the set upper and lower limits of the CV cycle.

levels of degradation were incited on the electrode by the different CV potential limits. The electrodes were characterized and imaged before and after the degradation. A total of 13 electrodes were degraded, with 3 electrodes for each of the 4 experimental conditions. To illustrate an extreme case of damage, one electrode was exposed to a very high potential limit window. The experimental details for the degradation protocol are described in table 4. Each electrode was degraded at regular chronological intervals, for instance, each nominal case potential cycling was performed every 3 h. The reason for such periodic scheduling was to include the effect of the electrode exposure to saline for long durations.

6.1.1. Note on degradation protocol

We have seen from preliminary experiments done *in vivo* in section 5, that in the absence or failure of charge balancing mechanisms, RV can grow to exceed water window levels, which can lead to electrode damage. A degradation protocol was designed to introduce some damage to the electrode–electrolyte interface. While the protocol does not aim to characterize the exact mechanisms that lead to degradation in typical stimulation scenarios, it accelerates voltage damage at the electrode–electrolyte interface. Using CV we were able to systematically repeat the same degradation profile for several electrodes, at different levels, and induce damage within a short time. The

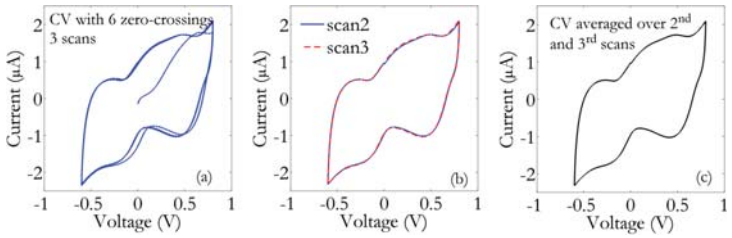

Figure 10. CV Averaging Example: (a) CV response with six zero crossings (b) extracted two scans (2,3) from the full CV curve shown in (a) and (c) average CV curve from the two curves shown in (b). The first scan is removed because it corresponds to a non-steady state. The curve shown in (c) is typically reported for this work and is used for calculating the cathodal charge storage capacity.

types of damage that were observed were cracking of the electrode surface, corrosion and delamination. It must also be noted that the experiments performed in this paper to validate the usefulness of RV were demonstrated with a single type of electrode, i.e. SIROF, other electrodes may exhibit different mechanisms of damage. The results and images described in section 7.3 will elucidate the different types of damage achieved through the use of the protocol, and discuss how RV can be used to detect some of these changes.

6.2. Imaging

Preliminary optical imaging of the electrodes to view the systematic degradation was done using the ScopeTek MD560 Digital Microscope. To study the nature of degradation, the electrodes were imaged using an environmental scanning electron microscope (eSEM). An eSEM allows the collection of electron micrographs of specimens that are uncoated (non-conducting), by allowing a relatively high pressure in the specimen chamber. The eSEM model used was the Quanta 200 (FEI, OR, USA).

7. Results and discussion

For the 13 electrodes that were subject to the degradation protocol described in table 4, biphasic responses were obtained for all electrodes before and after applying the protocol. All the electrodes (three electrodes per degradation category) were also characterized by CV and EIS, before and after the application of the degradation protocol.

7.1. Pre-degradation characterization

Stimulation electrodes are typically characterized by their cathodal charge storage capacity. Cathodal charge storage capacity is calculated by numerically integrating the area enclosed by the negative Y-axis curve of a CV plot. CV plots consist of multiple zero-crossings, as shown in figure 10(a). In this work, a total of six zero-crossings were used for a typical characterization, which implies there are three complete CV scans. While the first scan was omitted because the response is in a non-steady state, to calculate the charge storage capacity, the second and third scans were averaged (figure 10(b)) and the cathodal charge storage capacity was obtained from figure 10(c). Henceforth, all CV plots reported in this paper are averaged CV plots. The break-in procedure for SIROF electrodes (described in section 4.2) involves potential cycling the electrode between the water window limits. This process increases the real surface area of the SIROF material, thereby increasing the charge storage capacity. The averaged CV scans for all electrodes before applying the degradation protocol are shown in figure 11(b).

The average transient biphasic response for 13 electrodes *before* degradation is shown in figure 11(a). The step increase in the electrode voltage corresponds to the ohmic response of the solution resistance, R_s, and the slope refers to the charging mechanism of the double-layer capacitance, C_{dl}, as well as the discharging across the charge-transfer resistance, R_{ct} (to first order).

Electrode–electrolyte interfaces are characterized by EIS in order to determine the impedance characteristics. The mean and error of the EIS Bode plots (magnitude and phase) for the electrochemical impedance of all the electrodes before applying the degradation protocol are shown in figure 11(c). The potential cycling of the SIROF material activates it, which increases the real surface area of the electrode and hence increases the double-layer capacitance. An increase in the capacitance shows a decrease in the low frequency impedance in figure 11(c).

7.2. Degradation protocol

The degradation protocol described in table 4 was applied on a total of 13 electrodes, with 3 electrodes each for protocols DP-I to DP-IV, and one electrode for DP-V because it was an extreme case. CV plots demonstrating each condition are shown in figure 12. As the voltage range increases, the current conducted across the interface increases by more than one order of magnitude. The degradation procedure was used primarily to *alter* the characteristics of the electrode–electrolyte interface,

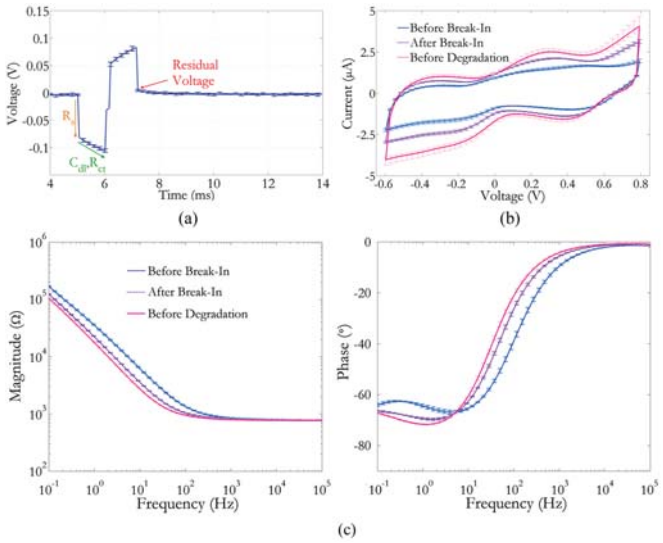

Figure 11. Characterization plots before degradation protocol: (a) biphasic transient response of SIROF electrode array: the graphs shows the mean of the transient biphasic response of 13 electrodes #3–#15, along with error bars for different time points (downsampled for clarity), with a maximum voltage error range of 80mV. (b) CV plots: the data here show the mean and error for the averaged CV cycle (figure 10) for electrodes #3–#15. The break-in of the electrodes by potential cycling activates the iridium oxide, thereby increasing the charge storage capacity of the electrodes (section 4.2). (c) EIS Bode plots: the data here show the mean and error of the magnitude and phase plots for electrodes #3–#15. The break-in of the electrodes by potential cycling activates the iridium oxide, increasing the capacitance, thereby decreasing the low-frequency impedance on the magnitude plot.

to study RV measurements on altered stimulation electrodes.

7.3. Post-degradation protocol results

7.3.1. eSEM imaging

Low vacuum scanning electron microscope (eSEM, 50 000X magnification) images of the electrodes after the degradation protocol. The protocol enabled the creation several degraded electrode modes, such as corrosion, mechanical damage, re-deposition and delamination, which are shown and described in figure 13.

7.3.2. Biphasic transient responses

A comparison of the biphasic responses and CV characterization for each of the degraded electrodes is shown in figure 14. Recall that the biphasic stimulation pulse is a rectangular current pulse (figure 1(a)). When a rectangular current pulse passes through a capacitor (C_{dl}), the resulting waveform is a straight line, with a slope of $(1/C_{dl})$. Therefore, a decrease in the slope of the biphasic response, indicates an increase in the double-layer capacitance to first order, which can be observed in figures 14(c)–(f). The electrodes subject to DP-IV, which mainly exhibit surface delamination, i.e. a significant loss of the the SIROF material coating, show a drastic reduction in the charge storage capacity thereby increasing the amplitudes of the biphasic response, and subsequently the RV.

RV can theoretically be sampled at any point after the biphasic pulse, constrained only by the measurement circuit. Here, we present two cases, figure 15(a) shows the values of the RV 1 μs and figure 15(b) shows the values 1 ms after the anodic phase, for the electrodes before and after the degradation protocol. Smaller C_{dl} values, which are apparent in the case of surface delamination, correspond to a higher RV, which is evident from the RV sampled after 1 μs (figure 15(a)). The later the measurement is made, as shown in figure 15(b), the harder it becomes to distinguish between the degraded cases due to noise interference.

7.3.3. Charge storage capacity

As described in section 4, the cathodal charge capacity (C cm^{-2}) was obtained by integrating under the negative half of the CV curve, and dividing it by the geometric area of the electrode. While a gradual transition can be observed across the samples from initial use until degradation (figure 16), there is a distinct reduction in cases where the SIROF film has significantly delaminated. For electrodes tested with degradation protocols DP-I (#5,#10,#15) and DP-II (#3,#4,#6), which are within and at the water window limits, an increase in charge storage capacity is observed (figure 16), without a significant change in the surface topology (figures 13(b) and (c)). For DP-III (#7,#8,#9), the damage is more pronounced, causing visible cracking on the surface

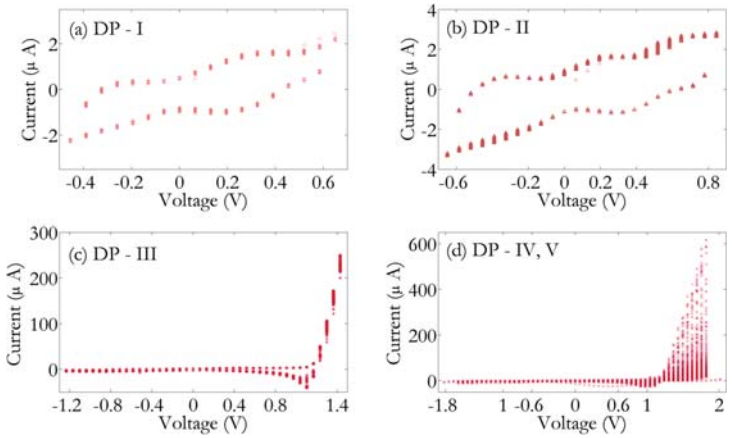

Figure 12. CV-based electrode DP: CV cycles were run at limits higher than the specified water window potentials (−0.6/+0.8V for SIROF [23]) to ensure systematic, repetitive and expeditious changes in the electrode–electrolyte interface characteristics (ref table 4) (a) DP I (Nominal) (b) DP II (At Water Window) (c) DP III (|0.6V| Above Water Window) (d) DP IV (|1V| Above Water Window). As the applied voltages increases, the conduction across the electrode–electrolyte interface increases due to irreversible electrochemical reactions, thereby damaging the electrode.

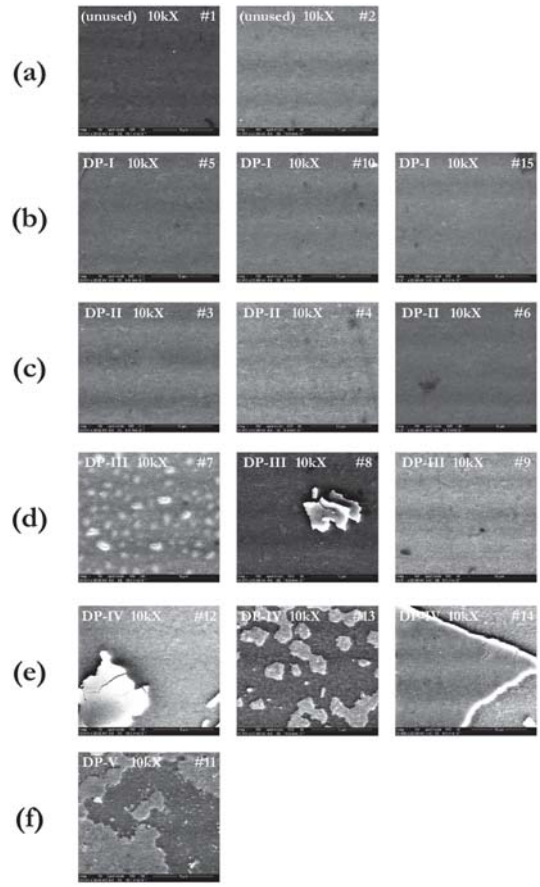

Figure 13. ESEM images after Degradation Protocol (DP, table 4) 10kX magnification: (a) unused electrodes showing the general structure of SIROF film (b) DP—I, nominal voltage range, within the water window, there is no significant texture change in all electrodes (c) DP—II, operated at the water window limits, cracks start to appear on the surface (d) DP—III, operated above the water window, the SIROF film starts to rupture (#7), #8 shows a redeposition of SIROF film, these cases can exhibit an increase in charge storage capacity, #9 shows an absence of SIROF film (e) DP—IV, operated above the water window, shows delamination, resulting in absence of SIROF material in most areas, #12, #13 shows absence of SIROF film (f) DP—V, test case for very high voltage range, resulting in delamination.

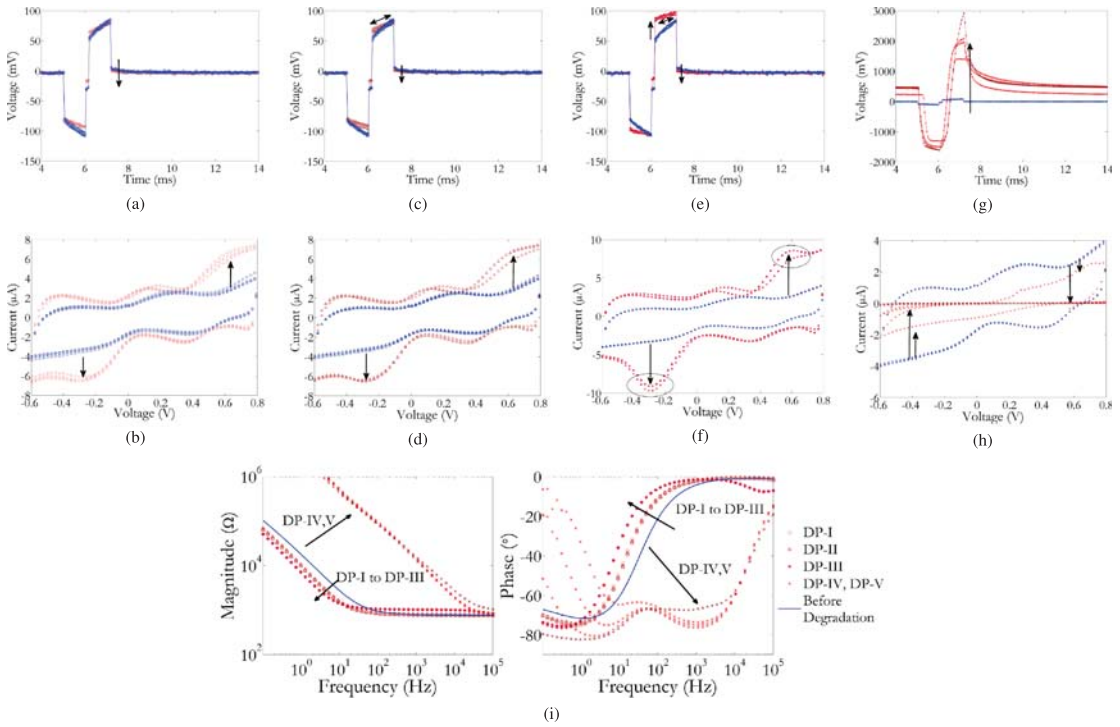

Figure 14. Outcome of DP—Biphasic response and CV plots (a) and (b) DP-I, Nominal case within the water window (c) and (d) DP-II, at the water window. There is a noticeable decrease in the slope of the biphasic response, indicating an increase in the double-layer capacitance, corroborated by the increase in the enclosed area of the CV curve. (e) and (f) DP-III, above the water window by |0.6|V. There is an increase in the solution resistance, indicated by the step change in the biphasic response. The CV curve, while showing an increase in area, also shows a lot more electrochemical reactions, based on the sharp peaks at higher voltage ranges. Surface cracking exhibited in figure 13(d) can exhibit an increase in the real surface area. (g),(h), above the water window by |1|V, indicating large RV values for electrodes where surface delamination is predominant. (i) EIS Bode plots after DP: The solid blue line shows the mean plot from all electrodes before degradation. For protocols DP-I, DP-II and DP-III, there is no significant change in the magnitude plot between them, but they decrease from the pre-degraded response. The degraded cases, DP-IV and DP-V show a large increase in impedance, corresponding to a large increase in residual voltage measurement.

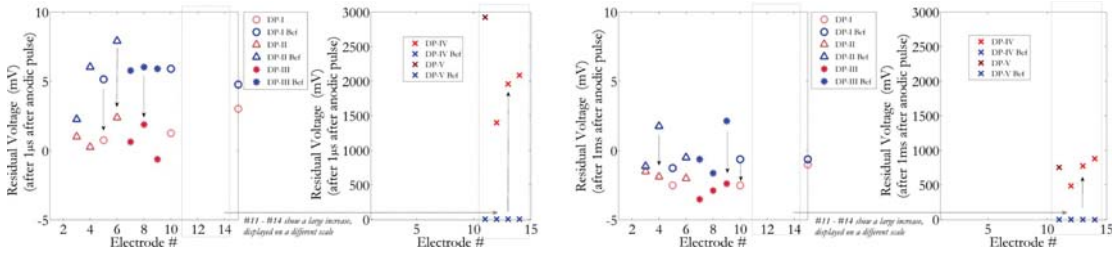

(a) Post Degradation: Residual Voltage after $1\mu s$ after the anodic pulse

(b) Post Degradation: Residual Voltage after $1ms$ after the anodic pulse

Figure 15. Post degradation: RV measurement (a) measured after 1 μs (b), after the anodic pulse: an increase in charge storage capacity (shown in figure 16) indicates a decrease in RV measurement. Measurement of RV further away in time from the end of the anodic pulse is more prone to noise interference.

(figure 13(d)), and redeposition of SIROF material. This case is interesting because it causes an *increase* in the charge storage capacity, but this increase is not a reliable feature. If there is a large deviation from the standard charge storage capacity, a *decrease* in RV can imply cracking on the electrode surface. For the last case of complete delamination, at that point, there is no SIROF material remaining, which decreases the capacitance significantly.

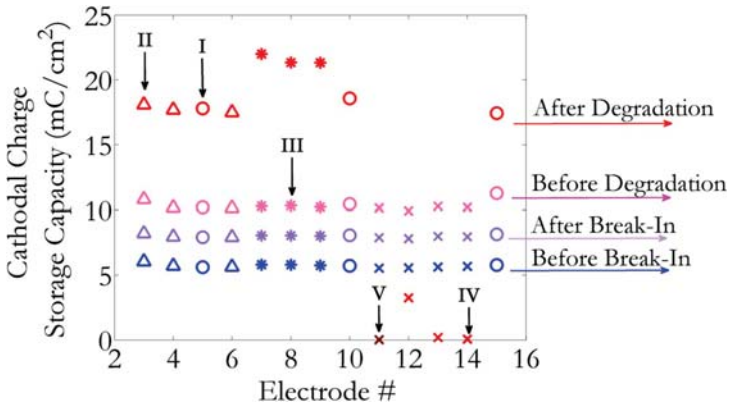

Figure 16. Cathodal charge storage capacity response: The figure shows the cathodal charge storage capacity for the electrodes before and after applying our degradation protocol. Initially, the electrodes exhibit a mean charge storage capacity of 5.7 mC cm^{-2}. All the electrodes were subject to potential cycling for 60 minutes at voltage ranges described in table 4. The potential cycling increases the charge storage capacity, indicating an increase in the value of the double-layer capacitor. Damaged electrodes, however, show a drastic reduction in charge storage capacity, due to delamination of the SIROF electrode. The degradation procotol (DPI-V) is marked with a different color, but is considered as a case of SIROF film delamination.

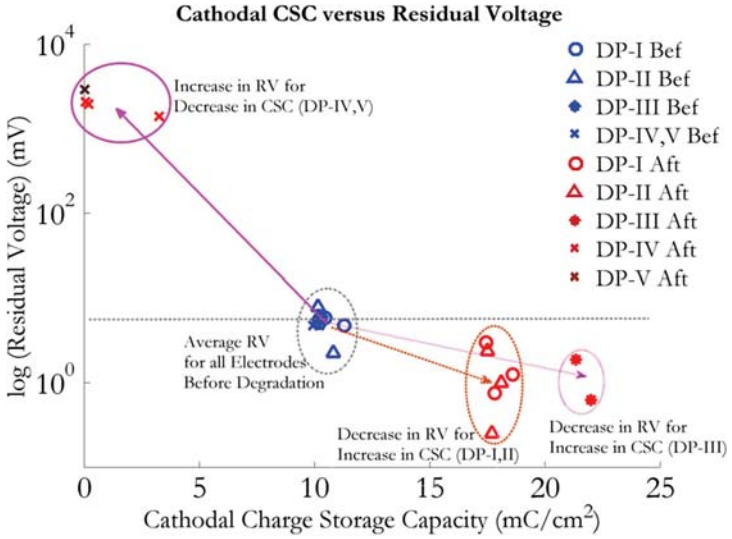

Figure 17. Scatter plot of cathodal charge storage capacity versus the log RV measure after 1 μs. A decrease in cathodal charge storage capacity shows an increase in RV, and vice versa.

8. Conclusion

RV is a leakage phenomenon that can occur during perfectly balanced biphasic electrical stimulation due to discharge of the double-layer capacitance via the charge-transfer resistance. Because it is representative of the condition of the electrode–electrolyte (tissue) interface, measurement of RV is a useful tool to monitor changes that occur at the interface. Stimulation electrodes are typically coated with an electrochemically active material, like iridium oxide, in order to enhance their charge injection capacity. The charge-transfer resistance in the first-order model represents the electrochemical reactions that take place across the interface. Using a first-order model of the electrode–electrolyte (tissue) interface, we describe the source of RV in balanced biphasic electrical stimulation. Using electrochemical analysis methods such as CV and EIS, and comparing against RV measurements, we demonstrate the correlation between RV measurement and electrode damage. While the values presented in this paper have used SIROF electrodes as a proof-of-concept, different systems may present different values, but the concept of measuring RV remains unchanged. Our motivation for including RV measurement in any closed loop neuromodulation system is evident from *in vivo* experiments performed in rats showing how uncurtailed RV grows to levels that are beyond the electrochemical water window.

From our studies presented in this paper, we are able to draw the following conclusions: (a) RV is present even when the biphasic stimulation is perfectly charge balanced; (b) there is evidence to

suggest that cases of electrode cracking or delamination of SIROF electrodes can be detected by RV measurements during stimulation. A decrease in the charge storage capacity corresponds to an increase in the measured RV (figure 17); (c) RV measurements should preferably be done as close in time to the end of the anodic phase as possible, in order to ensure a reliable demarcation between nominal and degraded cases; (d) preliminary *in vivo* experiments in anesthetized rats show evidence that RV growth can grow beyond the water window limits.

The *in vivo* RV growth to water window levels occurs in a short time frame (40 min), and the average life of a chronic implant device is a few years. A lot of physiological effects in biological systems only occur on chronic exposure, which can be more than 7 h. A future direction of this work would be to observe (a) RV variations in different types of stimulation electrodes and at different charge densities and (b) long term electrode degradation of electrodes implanted *in vivo*, while simultaneously observing RV measurements. From a system design standpoint, the fact that RV exists even with zero charge mismatch implies system design effort can be split between minimizing mismatch and developing feedback based charge balancing methods. On the other hand, implementation of existing charge balancing methods [16, 19], can incorporate these ad-hoc RV measurements to ensure that unwanted voltages do not linger at the electrode node, while still retaining valuable diagnostic information in the process of charge balancing. In applications involving implantable electronics, where *in situ* characterizations using traditional CV and electrode impedance spectroscopy methods can often be inaccessible, we present RV measurement as an efficient and scalable way of diagnosing discrepancies in multi-electrode systems.

Data availability statement

The data that support the findings of this study are available upon reasonable request from the authors.

Acknowledgement

Research reported in this publication was supported by the Dept. of Veterans Affairs grant I01-RX000506, National Institute of Neurological Disorders and Stroke of the National Institutes of Health under Award Number R01NS089668 and NS110564.

ORCID iDs

Ashwati Krishnan https://orcid.org/0000-0002-9229-1639
Mats Forssell https://orcid.org/0000-0001-7811-6773
Zhanhong Du https://orcid.org/0000-0001-6535-1424
X Tracy Cui https://orcid.org/0000-0002-0470-2005
Gary K Fedder https://orcid.org/0000-0002-2380-5210
Shawn K Kelly https://orcid.org/0000-0003-3533-5268

References

[1] Nolta N F, Christensen M B, Crane P D, Skousen J L and Tresco P A 2015 BBB leakage, astrogliosis and tissue loss correlate with silicon microelectrode array recording performance *Biomaterials* **53** 753–62
[2] Barrese J C, Rao N, Paroo K, Traibwasser C, Vargas-Irwin C, Franquemont L and Donahue J P 2013 Failure mode analysis of silicon-based intracortical microelectrode arrays in non-human primates *J. Neural Eng.* **10** 6
[3] Merrill D R and Tresco P A 2005 Impedance characterization of microarray recording electrodes in vitro *IEEE Trans. Biomed. Eng.* **52** 1960–5
[4] Negi S, Bhandari R, van Wagenen R and Solzbacher F 2010 Factors affecting degradation of sputtered iridium oxide used for neuroprosthetic applications *IEEE 23rd Int. Conf. on Micro Electro Mechanical Systems*
[5] Cogan S F, Ludwig K A, Welle C G and Takmakov P 2016 Tissue damage thresholds during therapeutic electrical stimulation *J. Neural Eng.* **13** 2
[6] Shannon R V 1992 A model for safe levels of electrical stimulation *IEEE Trans. Biomed. Eng.* **39** 424–6
[7] Lilly J C, Hughes J R, Alvord E C Jr and Galkin T W 1955 Brief, noninjurious electric waveform for stimulation of the brain *Science* **121** 468–9
[8] Jose V J and Ghovanloo M 2010 Towards a switched-capacitor based stimulator for efficient deep-brain stimulation *IEEE Engineering in Medicine and Biology Conf* pp 2927–30
[9] Liu X, Demostheous A and Donaldson N 2008 In vitro evaluation of a high-frequency current-switching stimulation technique for FES applications *13th Conf. Int. Functional Electrical Stimulation Society* pp 291–3
[10] Kelly S and Wyatt J 2011 A power-efficient neural tissue stimulator with energy recovery *IEEE Trans. Biomed. Circuits Syst.* **5** 20–9
[11] Rattay F 1989 Analysis of models for extracellular fiber stimulation *IEEE Trans. Biomed. Eng.* **36** 674–82
[12] Hughes M L, Choi S and Glickman E 2018 What can stimulus polarity and interphase gap tell us about auditory nerve function in cochlear-implant recipients? *Hear. Res.* **359** 50–63
[13] Weitz A C *et al* 2014 Interphase gap as a means to reduce electrical stimulation thresholds for epiretinal prostheses *J. Neural Eng.* **11** 1
[14] Davidovics N S, Fridman G Y, Chiang B and Santina C C D 2011 Effects of biphasic current pulse frequency, amplitude, duration and interphase gap on eye movement responses to prosthetic electrical stimulation of the vestibular nerve *IEEE Trans. on Neural Systems and Rehabilitation Engineering* **19** 1
[15] Merrill D R, Bikson M and Jefferys J G R 2005 Electrical stimulation of excitable tissue: design of efficacious and safe protocols *J. Neurosci. Methods* **141** 171–98
[16] Krishnan A and Kelly S 2012 On the cause and control of residual voltage generated by electrical stimulation of neural tissue *IEEE Engineering in Medicine and Biology Conf.* pp 3899–902

[17] Krishnan A and Kelly S 2015 On using residual voltage to estimate electrode model parameters for damage detection *IEEE Biomedical Circuits and Conf.*
[18] Aryan N P, Kaim H and Rothermel A 2015 *Charge Balance and Safe Operation Conditions* (Berlin: Springer) pp 17–23
[19] Sooksood K, Stieglitz T and Ortmanns M 2010 An active approach for charge balancing in functional electrical stimulation *IEEE Trans. Biomed. Circuits Syst.* **4** 162–70
[20] Cogan S F *et al* 2004 Sputtered iridium oxide films (SIROFs) for neural stimulation electrodes *IEEE Engineering in Medicine and Conf.* vol 6 pp 4153–6
[21] Krishnan A and Kelly S K 2016 Residual voltage in biphasic electrical stimulation: cause, clues, and control PhD Dissertation Carnegie Mellon University, Pittsburgh, PA
[22] Shire D B *et al* 2009 Development and implantation of a minimally invasive wireless subretinal neurostimulator *IEEE Trans. Biomed. Eng.* **56** 2502–11
[23] Cogan S F 2008 Neural stimulation and recording electrodes *Annu. Rev. Biomed. Eng.* **10** 275–309
[24] Mozota J and Conway B E 1983 Surface and bulk processes at oxidized iridium electrodes – I. Monolayer stage and transition to reversible multilayer oxide film behaviour *Electrochim. Acta* **28** 1–8